Synthetic and Systems Biotechnology 10 (2025) 102–109

Contents lists available at ScienceDirect

Synthetic and Systems Biotechnology

journal homepage: www.keaipublishing.com/en/journals/synthetic-and-systems-biotechnology

Original Research Article

Functional investigation of the SAM-dependent methyltransferase RdmB in anthracycline biosynthesis

Moli Sang [a,b], Qingyu Yang [a,b], Jiawei Guo [a,b], Peiyuan Feng [a,b], Wencheng Ma [a,b], Wei Zhang [a,b,c,*]

[a] State Key Laboratory of Microbial Technology, Shandong University, Qingdao, Shandong, 266237, China
[b] Shenzhen Research Institute of Shandong University, Shenzhen, 518057, China
[c] Laboratory for Marine Biology and Biotechnology, Qingdao Marine Science and Technology Center, Qingdao, Shandong, 266237, China

ARTICLE INFO

Keywords:
Methyltransferase
Anthracyclines
Biosynthesis
Catalytic mechanism

ABSTRACT

A novel sub-class of *S*-adenosyl-L-methionine (SAM)-dependent methyltransferases catalyze atypical chemical transformations in the biosynthesis of anthracyclines. Exemplified by RdmB from *Streptomyces purpurascens,* it was found with 10-decarboxylative hydroxylation activity on anthracyclines. We herein investigated the catalytic activities of RdmB and discovered a previously unknown 4-*O*-methylation activity. The site-directed mutagenesis studies proved that the residue at position R307 and N260 are vital for the decarboxylative hydroxylation and 4-*O*-methylation, respectively, which define two distinct catalytic centers in RdmB. Furthermore, the multifunctionality of RdmB activity was found as cofactor-dependent and stepwise. Our findings expand the versatility and importance of methyltransferases and should aid studies to enrich the structural diversity and bioactivities of anthracyclines.

1. Introduction

Anthracyclines, exemplified by doxorubicin, aclacinomycin A, and epirubicin, constitute an important class of anti-tumor chemotherapeutic drugs with a broad spectrum of anticancer activity (Fig. S1) [1–4]. A novel sub-class of SAM-dependent methyltransferases play important roles in the bioactivity and structural diversity of anthracyclines by catalyzing atypical chemical transformations [1,5,6]. Biosynthetically, anthracyclines are derived from type II polyketide synthases and feature a tetracyclic 7,8,9,10-tetrahydro-5,12-naphtacenoquinone scaffold, which is further modified by post-modification enzymes with unconventional reactions [1,7,8].

The *S*-adenosyl-L-methionine-dependent methyltransferase (MT) RdmB from the *β*-rhodomycin biosynthesis in *Streptomyces purpurascens* has significantly atypical functions [5,9,10]. Previous studies have revealed that RdmB acts as 10-hydroxylase to catalyze a decarboxylative hydroxylation reaction on anthracyclines, but without displaying methyltransferase activity (Fig. S2) [5,6,11,12]. Interestingly, the hallmark *C*-terminal *S*-adenosyl-L-methionine (SAM-binding) motif GxGxG of MTs is found with RdmB by protein sequence analysis (Fig. S3), and the Class I Rossman-like fold is observed with highly similar to that of classical SAM-dependent MTs (*i.e.,* DnrK) by crystal structure comparisons [10,11,13]. Thus, it's of particular curious to aware why a structurally typical MT does not have the catalytic activity that is characteristic of it.

During our investigating of the catalytic basis for the functions of RdmB, we discovered for the first time of the 4-*O*-methylation activity of RdmB. The incubation of RdmB and the substrate 10-carboxy-13-deoxycarminomycin (**1**) *in vitro* in the presence of SAM, the expected 10-hydroxylation product 10-hydroxyl-13-deoxycarminomycin (**2**), together with the 4-*O*-methylated product **3** was steadily produced. These results clearly demonstrated that RdmB is able to catalyze the methylation reaction as a conventional SAM-dependent *O*-methyltransferase, in addition to its hydroxylation activity. The site-directed mutagenesis studies revealed that the residue at position R307 and N260 are involved in the 10-hydroxylation and 4-*O*-methylation, respectively. Furthermore, RdmB catalyzed methylation and decarboxylative hydroxylation in a cofactor-dependent and stepwise mechanism by time-dependent study.

Peer review under responsibility of KeAi Communications Co., Ltd.
* Corresponding author. State Key Laboratory of Microbial Technology, Shandong University, Qingdao, Shandong, 266237, China.
E-mail address: zhang_wei@sdu.edu.cn (W. Zhang).

https://doi.org/10.1016/j.synbio.2024.09.002
Received 27 July 2024; Received in revised form 30 August 2024; Accepted 6 September 2024

2. Methods

2.1. Materials

10-carboxy-13-deoxycarminomycin (**1**) is isolated from *S. coeruleorubidus::*ΔDnrK mutant strain, which is an analog of 15-demethoxy-ε-rhodomycin and identified as a biosynthetic intermediate of daunorubicin. It was [14,15]. Compounds **2** and **3** were obtained through enzymatic reactions. SAM (*S*-adenosyl-L-methionine) and SAH (*S*-adenosine-L-homocysteine) were purchased from Aladdin (Shanghai, China), and sinefungin was purchased from Psaitong (Beijing, China). All antibiotics used in this study were obtained from Solarbio (Beijing, China). All restriction enzymes were purchased from Thermo Scientific (PA, USA). 2 × Phanta Max Master Mix Vazyme (Nanjing, China) was employed to amplify DNA fragments. Kits for plasmid mini-preparations and DNA gel extractions were acquired from Omega Bio-tek, Inc. (GA, USA). Ni-NTA SefinoseTM Resin (Settled Resin) for protein purification was purchased from Sangon Biotech (Shanghai, China). The FlexiRun premixed gel solution for SDS-PAGE was obtained from MDBio (Qingdao, China). Oligonucleotide primers and DNA sequencing were ordered from TsingKe Biotech (Shanghai, China). Gene synthesis was ordered from Beijing Genomics Institution (Shenzhen, China). Organic solvents for compound isolation and purification were bought from sinopharm (Shanghai, China).

2.2. Analytical procedures

The protein sequence alignments were performed using T-Coffee [16] and ESPript3 [17]. NMR data were processed using MestReNova 9.0. All HPLC (Dionex Ultimate 3000 instrument) analyses were performed on a YMC Triart C18 column (4.6 × 250 mm, 5 μm, UV detection at 470 nm) with a biphasic solvent system of acetonitrile-0.1 % formic acid (solvent B) and water (solvent A) at a flow rate of 1.0 mL/min. All UPLC (Acquit-H-class, Waters) analyses were performed using a YMC Triart C18 (2.1 × 100 mm, 1.9 μm, UV detection at 470 nm) column with a biphasic solvent system of acetonitrile-0.1 % formic acid (solvent B) and water (solvent A) at a flow rate of 0.4 mL/min. HRESI-LCMS analyses were carried out on a Bruker impact HD High Resolution Q-TOF mass spectrometer.

2.3. Strain and culture conditions

S. coeruleorubidus and mutant were grown in NDYE liquid medium (maltose 22.5 g, yeast extract 5.04 g, $NaNO_3$ 4.28 g, K_2HPO_4 0.23 g, HEPES 4.77 g, $MgSO_4{\cdot}7H_2O$ 0.12 g, NaOH 0.4 g, 1 L; adding trace element solution: $ZnCl_2$ 40 mg, $FeCl_3{\cdot}6H_2O$ 200 mg, $CuCl_2{\cdot}2H_2O$ 10 mg, $MnCl_2{\cdot}4H_2O$ 10 mg, $Na_2B_4O_7{\cdot}10H_2O$ 10 mg, $(NH_4)_6Mo_7O_{24}{\cdot}4H_2O$ 10 mg, 1 L) or on MS agar (soybean flour 20 g, mannitol 20 g and agar 20 g, 1 L) plates at 30 °C for 5 days. *Escherichia coli* DH5α strain was used for vector construction and plasmid preparation. *E. coli* BL21(DE3) (for *N*-His^6-tagged proteins) was used for protein expression, and cultured in LB media.

2.4. Construction of gene inactivation mutants

The CRISPR/Cas9 genome editing technology was used for gene *dnrK* disruption [18]. To construct the plasmid for the target gene inactivation, the upstream and downstream homology arms were amplified with dnrK-LF/dnrK-LR primers and dnrK-RF/dnrK-RR primers using genomic DNA of *S. coeruleorubidus* as template. The *dnrK* deletion sgRNA expression cassette was amplified from pKCcas9dO with the dnrK-sgRNA-F/dnrK-sgRNA-R primers. The above three fragments were then ligated to the plasmid pKCcas9dO, which was linearized by *SpeI* and *HindIII* using the ClonExpress Ultra One Step Cloning Kit to construct the knockout plasmid pKCcas9d-dnrK. The plasmid was then conjugated into S. *coeruleorubidus* according to the standard procedure [19]. After cultured for 3–5 days at 30 °C, the colonies with apramycin-resistant were transferred to MS plates supplied with apramycin antibiotics at final concentration of 100 μg/mL. The apramycin-sensitive colonies were picked and confirmed by diagnostic PCR analysis using the primers dnrK-VF/dnrK-VR. Wild type *S. coeruleorubidus* st was used as a control and the expected lengths of the PCR products were 2706 bp and 1635 bp, respectively. Subsequently, mutant *S. coeruleorubidus::*ΔDnrK was cultured on MS plates without any antibiotics at 37 °C to lose the CRISPR/Cas9 plasmids.

2.5. Isolation of 10-carboxy-13-deoxycarminomycin (1)

To characterize the accumulated compounds of the mutant strain *S. coeruleorubidus::*ΔDnrK, a 1 L fermentation was carried out for the mutant strain ΔDnrK using the fermentation condition described above. After 5 days of cultivation, the fermentation broth was collected and dried under vacuum to obtain crude extracts. The crude extracts were subjected to HPLC for purification **1** using a YMC Triart C18 column (20 mm × 250 mm, 7 μM). Water (solvent A) and acetonitrile-0.1 % FA (solvent B) were used as the mobile phases at a flow rate of 15 mL/min. The HPLC program was as follows: 0–2 min, 20 % B in A; 2–20 min, 20–80 % B in A; 20–20.5 min 80–100 % B in A; 20.5–22 min 100 % B; 22–22.5 min 100-20 % B in A; and 22.5–25 min 20 % B in A. The obtained fractions were dried under vacuum to give compounds **1** (63 mg), whose structures were identified by HRESI-LCMS and NMR analysis.

2.6. Construction of plasmids for protein expression

The site-specific mutations of RdmB were constructed by site-directed PCR using PET28a-*rdmB* as template using primer pairs of $RdmB^{3GA}$-F/$RdmB^{3GA}$-R, $RdmB^{N260A}$-F/$RdmB^{N260A}$-R, and $RdmB^{R307A}$-F/$RdmB^{R307A}$-R. The individual amplified product was purified using the Omega Gel Extraction Kit according to the manufacturer's instructions and then transformed into *E. coli* DH5α for plasmid amplification. The above recombinant plasmids were verified by DNA sequencing and the correct plasmids were transformed into *E. coli* BL21 (DE3) for protein overexpression.

2.7. In vitro enzymatic assays and products detection

Unless otherwise stated, all enzymatic assays were carried out in a total volume of 100 μL in the desalting buffer (50 mM NaH_2PO_4, 300 mM NaCl, 10 % glycerol, pH 7.4) at 30 °C, and the boiled enzymes were used as negative controls. 0.1 mM **1** or **2** or **5** was incubated with 2 μM RdmB and 1 mM SAM at 30 °C for 2 h. To analyze the activity of RdmB mutants, RdmB was replaced by its mutants ($RdmB^{3GA}$/$RdmB^{N260A}$/$RdmB^{R307A}$) in the above reaction system. The reactions were quenched by thorough mixing with 200 μL methanol to precipitate the proteins. The metamorphosed proteins were removed by high-speed centrifugation at 14,000 rpm for 10 min, and the supernatants were analyzed by UPLC or HRESI-LCMS using gradient elution programs. Water-0.1 % FA (solvent A) and acetonitrile-0.1 % FA (solvent B) were used as the mobile phases. The UPLC program: 0–0.5 min, 20 % B in A; 0.5–5 min, 20–90 % B in A; 5–5.1 min 90–100 % B in A; 5.1–5.6 min 100 % B; 5.6–5.7 min 100-20 % B in A; and 5.7–6.5 min 20 % B in A at a flow rate of 0.4 mL/min, UV 470 nm. HRESI-LCMS program: 0–2 min, 20 % B in A; 2–20 min, 20–80 % B in A; 20–20.5 min 80–100 % B in A; 20.5–22 min 100 % B; 22–22.5 min 100-20 % B in A; and 22.5–25 min 20 % B in A at a flow rate of 1 mL/min, UV 470 nm.

2.8. The steady-state kinetic analysis of RdmB

The reactions of RdmB were carried out in 1.5 mL centrifugation tubes. The reaction containing RdmB (0.05–0.4 μM), 0.5 μM SAM and substrate **1** (10–150 μM) in 145 μL storage buffer (50 mM NaH_2PO_4, 10 % glycerol, pH 7.5) was incubated at 30 °C for 5 min. Then, the reactions

with different substrate concentration were initiated by adding the pre-incubated mixture of RdmB and SAM. The reaction was quenched at 0, 20, and 30 s by adding 50 μL of methanol. Samples were centrifuged at 14,000g for 10 min. The supernatant was subject to HPLC analysis (C18, 5 μm, 150 mm, Agilent 1220) to monitor substrate consumption. Water-0.1 % FA (solvent A) and acetonitrile-0.1 % FA (solvent B) were used as the mobile phases. The UPLC program: 0–7 min, 32 % B in A; 7–7.5 min, 32–100 % B in A; 7.5–9 min 100-100 % B in A; 9–9.5 min 100 % B; 9.5–12 min 100-32 % B in A; flow rate 1.0 ml/min, UV 470 nm. Kinetic analyses were performed using GraphPad Prism 8.3.0.

2.9. Time course analysis of the conversion of 1 catalyzed by RdmB

For the conversion of **1** by RdmB, a 100 μL reaction system containing 100 μM **1** with 2 μM RdmB in desalting buffer was incubated at 30 °C. The time points for the reactions were set to 0, 2, 5, 10, 30, 60, 120 min, respectively. When each reaction time point was reached, the reaction mixture was quenched with 200 μL methanol. After centrifugation at 14,000 rpm for 10 min, the supernatants were analyzed by UPLC, UV 470 nm. To investigate the conversion of **1** by RdmB with cofactor SAH or sinefungin, the reaction mixture containing 1 μM RdmB and 200 μM SAH or 200 μM sinefungin was incubated at room temperature for 10 min. Then, 50 μM **1** was added to the reaction mixture to initiate the enzymatic reaction (total volume was 300 μL). The time point for the reactions was set at 0, 2, 5, 10, 20, 30 min, respectively. When the reaction time point reached, a 50 μL aliquot of the reaction mixture was taken and quenched by mixing with 100 μL of methanol. After centrifugation at 14,000 rpm for 10 min, the supernatant was subjected to UPLC analysis. The reaction systems catalyzed by RdmB without additional cofactors were used as controls, following the same procedure as described above with the addition of cofactors (SAH and sinefungin). The consumption of **1** was estimated based on the standards. Error bars represent the standard deviation of three independent replicates.

2.10. Isolation of compound 2 and 3

To obtain sufficient of **2**, a 200 mL total volume large-scale enzymatic reaction were performed in desalting buffer containing 1 mM **1** and 5 μM RdmB. After incubation at 30 °C for 2 h, 400 mL of methanol was added to quench the reaction. Compound **3** (5 mg) was purified from the concentrated reaction mixture by semi-preparative HPLC using 24 % ACN in H_2O (0.1 % FA) at a flow rate of 3 mL/min.

To determine the structure of **3**, a 50 mL total volume large-scale enzymatic reaction was performed in desalting buffer containing 0.5 mM **2**, 10 μM RdmB, and 1 mM SAM. After incubation at 30 °C for 2 h, 100 mL of methanol was added to quench the reaction. Compound **3** (2 mg) was purified from the concentrated reaction mixture by semi-preparative HPLC using 26 % ACN in H_2O (0.1 % FA) at a flow rate of 3 mL/min.

2.11. NMR data of the compound 1-3

10-carboxy-13-deoxycarminomycin (**1**): ^{1}H NMR (600 MHz, MeOD) δ 7.82 - 7.63 (m, 1H), 7.60 (s, 1H), 7.28 - 7.07 (m, 1H), 5.43 (d, J = 9.5 Hz, 1H), 5.02 (d, J = 18.5 Hz, 1H), 4.27 (dd, J = 31.9, 6.4 Hz, 1H), 4.02 (d, J = 14.7 Hz, 1H), 3.65 (dd, J = 20.5, 9.9 Hz, 1H), 3.60 - 3.54 (m, 1H), 3.50 (dd, J = 11.2, 6.0 Hz, 1H), 2.48 - 2.35 (m, 1H), 2.27 (d, J = 13.5 Hz, 1H), 2.06 - 1.88 (m, 2H), 1.31 - 1.27 (m, 3H), 1.23 - 1.17 (m, 1H), 1.14 - 1.03 (m, 3H). ^{13}C NMR (151 MHz, MeOD) δ 187.67, 175.42, 168.82, 162.20, 160.31, 156.08, 136.79, 136.57, 133.29, 118.97, 118.81, 115.77, 115.69, 110.76, 110.50, 70.46, 66.56, 65.18, 63.01, 35.51, 34.23, 33.28, 30.51, 15.60, 6.21.

10-hydroxy-13-deoxycarminomycin (**2**): ^{1}H NMR (600 MHz, MeOD) δ 7.84 (s, 1H), 7.78 (s, 1H), 7.32 (s, 1H), 5.48 (s, 1H), 5.05 (s, 1H), 4.83 (s, 1H), 4.30 - 4.22 (m, 1H), 3.65 (d, J = 9.3 Hz, 1H), 3.58 (dd, J = 11.2, 4.9 Hz, 1H), 3.50 (dd, J = 11.2, 6.0 Hz, 1H), 2.17 (q, J = 14.8 Hz, 2H), 2.03 (t, J = 11.6 Hz, 1H), 1.89 (d, J = 9.2 Hz, 1H), 1.82 (dt, J = 14.6, 7.2 Hz, 1H), 1.79 - 1.71 (m, 1H), 1.29 (d, J = 6.5 Hz, 3H), 1.09 (t, J = 7.4 Hz, 3H). ^{13}C NMR (151 MHz, MeOD) δ 188.28, 171.68, 164.49, 163.52, 161.95, 139.17, 135.66, 130.47, 129.37, 126.46, 121.45, 121.20, 113.80, 113.42, 102.32, 74.55, 73.21, 68.66, 68.63, 67.06, 65.10, 34.78, 32.24, 30.29, 17.64, 7.60.

10-hydroxy-13-deoxydaunorubicin (**3**): ^{1}H NMR (600 MHz, MeOD) δ 8.06 (t, J = 11.0 Hz, 1H), 7.88 (t, J = 8.0 Hz, 1H), 7.61 (d, J = 8.3 Hz, 1H), 5.48 (d, J = 3.3 Hz, 1H), 5.07 (d, J = 2.8 Hz, 1H), 4.90 (s, 1H), 4.31 - 4.18 (m, 1H), 4.05 (s, 3H), 3.66 - 3.62 (m, 1H), 3.58 (dd, J = 11.2, 4.9 Hz, 1H), 3.50 (dd, J = 11.2, 6.0 Hz, 1H), 2.19 - 2.15 (m, 2H), 2.07 - 1.98 (m, 1H), 1.89 - 1.83 (m, 1H), 1.81 (dd, J = 14.0, 6.5 Hz, 1H), 1.74 (dd, J = 14.1, 7.3 Hz, 1H), 1.32 (dd, J = 14.3, 7.1 Hz, 2H), 1.28 (s, 3H), 1.09 (t, J = 7.4 Hz, 3H). ^{13}C NMR (151 MHz, MeOD) δ 187.75, 174.73, 163.32, 162.74, 158.19, 137.56, 136.72, 130.69, 129.34, 126.32, 121.32, 121.06, 114.41, 113.79, 102.39, 74.57, 73.44, 68.82, 68.62, 67.08, 65.13, 57.84, 34.80, 32.34, 30.39, 17.64, 7.59.

2.12. Confirmation of the presence of SAM in purified RdmB

300 μM RdmB in 30 μL storage buffer were denatured by heating at 100 °C for 10 min each. 100 μM SAM in water was heated at 100 °C for 10 min [20]. Then, the solutions were centrifuged at 14,000 rpm for 10 min. The supernatants were analyzed by HRESI-LCMS with a linear gradient of 5–60 % ACN-H_2O with 5 mM ammonium acetate in 25 min at a flow rate of 1 mL/min. UV detection was performed at 260 nm. The same procedures were performed for RdmB^{3GA}.

2.13. Crystallization, data collection and structure determination

Purified RdmB protein was mixed with both the respective **1** (100 mM stock in DMSO) and SAM (1 M stock in buffer) to a molar stoichiometry of 1:5:5 protein:**1**:SAM. Crystals were obtained by utilizing the sitting drop vapor diffusion method in a 1:1 ratio with the crystallization condition. The co-complex crystals of RdmB with 13-deoxydaunorubicin (DOD**)** were grown in the precipitating solution of 0.1 M Bis-Tris (pH 6.5), 2.0 M ammonium sulfate. Crystals were supplemented with cryo-protectants containing the reservoir contents plus 20 % ethylene glycol and flash-frozen in liquid nitrogen. Diffraction data of RdmB-DOD complex crystals were collected at 100 K on beamline BL18U at the Shanghai Synchrotron Radiation Facility (SSRF) and processed using the HKL3000 program [21].

2.14. Structure determination and refinement

The structure of RdmB-DOD was solved by molecular replacement, using the RdmB structure (PDB code: 1R00) structure as the search model. Further manual model building was facilitated by using Coot [22], combined with the structure refinement using Phenix [23]. The statistics of data collection and structure refinement are summarized in Table S3. The Ramachandran statistics, as calculated by Molprobity [24], are 97.70 %/1.02 % (favored/outliers) for structures of RdmB, respectively. All the structure diagrams were prepared using the ChimeraX 1.6.1 [25].

2.15. Molecular docking of substrate 1 to RdmB

To place the substrate into the active site of the RdmB, molecular docking of substrate **1** with and RdmB was performed using Autodock vina 1.2.0 [26], resulting in protein-substrate complex structures. Chem3D 19.0 was used to generate ligand **1**. The final structure of RdmB bound with **1** was selected based on the binding state of DOD in the RdmB co-crystal structure. After the protein-substrate complex structure was prepared, the substrate-protein interactions were analyzed using PLIP (the protein-ligand interaction profiler) (https://plip-tool.biotec.

tu-dresden.de) to determine key catalytic residues. Pymol and ChimeraX 1.6.1 were used for viewing the molecular interactions and image processing.

2.16. $^{18}O_2$ labeling experiments

To further verify the catalytic mechanism of RdmB, ^{18}O labeling $^{18}O_2$ (≥98 % labeled, Delin, Shanghai) were used to replace O_2 in the reaction system. The reaction was performed in a 100 μL reaction buffer using liquid bottle (2 mL). 2 μM RdmB was added to the reaction system, respectively. Then the bottle was purged with nitrogen and sealed with liquid bottle cap. $^{18}O_2$ was introduced into the bottle from the compressed gas bag via a syringe needle. Finally, 100 μM **1** was added to the bottle using a microsyringe. After incubation for 10 min at 30 °C, 100 μL methanol was added to stop the reactions. HRESI-LCMS analysis was carried out using the same method as above.

3. Results and discussion

3.1. Investigation of RdmB catalytic activity

Previous studies revealed that RdmB can recognize 15-demethoxy-ε-rhodomycin and 15-demethoxy-aclacinomycin T as substrate to catalyze only the SAM-dependent C-10 hydroxylation reaction [6,12]. To reinvestigate the functions of RdmB, which was expressed as a soluble *N*-terminal His^6-tagged protein (Fig. S4). RdmB-catalyzed reactions were conducted *in vitro* with substrate 10-carboxy-13-deoxycarminomycin (**1**) [14], an analog of 15-demethoxy-ε-rhodomycin, in the presence of SAM at 30 °C for 2 h (Fig. S5 and S20-24). UPLC and HRESI-LCMS revealed that the production of the expected 10-hydroxylation product 10-hydroxy-13-deoxycarminomycin (**2**, $[M+H]^+$: *obsd.* 516.1873, *calcd.* 516.1864) (Fig. 1a, 1b-ii, and Fig. S6), which was purified from a large-scale reaction and confirmed by 1D and 2D NMR analysis (Fig. S7 and S25-29). Unexpectedly, a new product **3** with a molecular mass of 530.2028 (*m/z*, $[M+H]^+$, *calcd.* 530.2021) was also detected by UPLC and HRESI-LCMS (Fig. 1a, 1b-i, and Fig. S6), indicating generation of a methylated product based on compound **2**. Further, when pure **2** was incubated with RdmB in the presence of SAM, **3** was produced with a high conversion rate and identified as 10-hydroxy-13-deoxydaunorubicin by 1D and 2D NMR analysis (Fig. S7, S8 and S30-34).

When the triglycosylated aclacinomycin A (AcmA) with the C-10 alkoxycarbonyl group was used as substrate, no methylated product of RdmB was detected in the presence of SAM, consistent with previous studies (Fig. S9) [6,10,12]. To further determine whether the presence of the C-10 alkoxycarbonyl or the triglycosyl group affects methylation activity, the monoglycosylated substrate rhodomycin D (RHOD) was incubated with RdmB [14]. Production of methylated rhodomycin D (4-*O*Me-RHOD) (Fig. S10) indicated that decarboxylation of the C-10 alkoxycarbonyl group is not a necessary step and that the triglycosyl group of anthracyclines prevents the methylation reaction. In addition, we investigated the methylation activity of RdmB using substrates that lacking the C-10 carboxyl group (13-deoxycarminomycin, DOC) [14]. The results revealed that in the presence of SAM, RdmB could catalyze the formation of the corresponding methylated products 13-deoxydaunorubicin (DOD) (Fig. S11). Thus, these results clearly demonstrated that RdmB can catalyze the methylation reaction as a conventional SAM-dependent *O*-methyltransferase in addition to its hydroxylation activity when the daunosamine glycosides of aklavinone were used as substrates.

Time-dependent production of **2** and **3** was discovered during time-course analysis of RdmB with **1** in the presence of SAM. Specifically, the conversion of **1** to **4** followed by the production of **2** was accomplished in 5 min with more than 90 % conversion rate by RdmB. With longer reaction time, conversion of **4** to **2** was observed. However, no methylated product **3** was detected until the reaction time was extended to 60 min (Fig. 2a and Fig. S12). Compound **4** was deduced to be a peroxide intermediate according to its *m/z* value (532.1822 $[M+H]^+$, *calcd.* 532.1813), which is 16 Da larger than that of **2** (Fig. S6). Further, when the RdmB-mediated reaction was performed in $^{18}O_2$, the molecular mass of **2** and **4** was increased by 2 Da and 4 Da, respectively (Fig. 2b–iii and

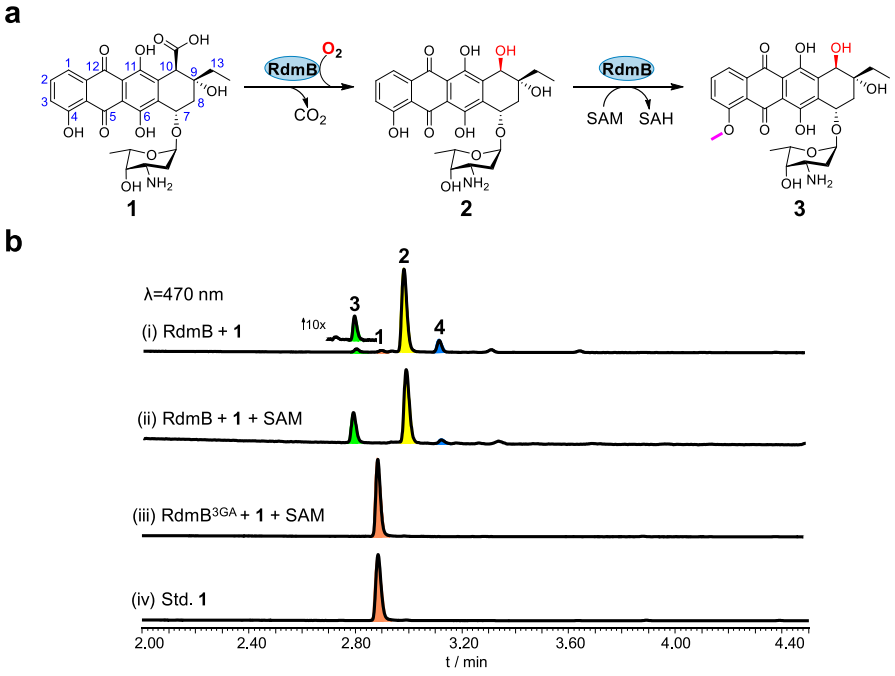

Fig. 1. The enzymatic conversion of **1** catalyzed by RdmB *in vitro*. (a) Reactions mediated by RdmB. Substrates and catalytic products: 10-carboxy-13-deoxycarminomycin (**1**), 10-hydroxyl-13-deoxycarminomycin (**2**), and 10-hydroxyl-13-deoxydaunorubicin (**3**). (b) UPLC analysis of the conversion of **1** catalyzed by RdmB and mutant RdmB^{3GA}. (i-iii) The conversion of **1** by (i) RdmB without additional cofactor SAM; (ii) RdmB in the presence of 1 mM SAM; (iii) RdmB^{3GA} in the presence of 1 mM SAM; (iv) Std. **1**: The standard of **1**.

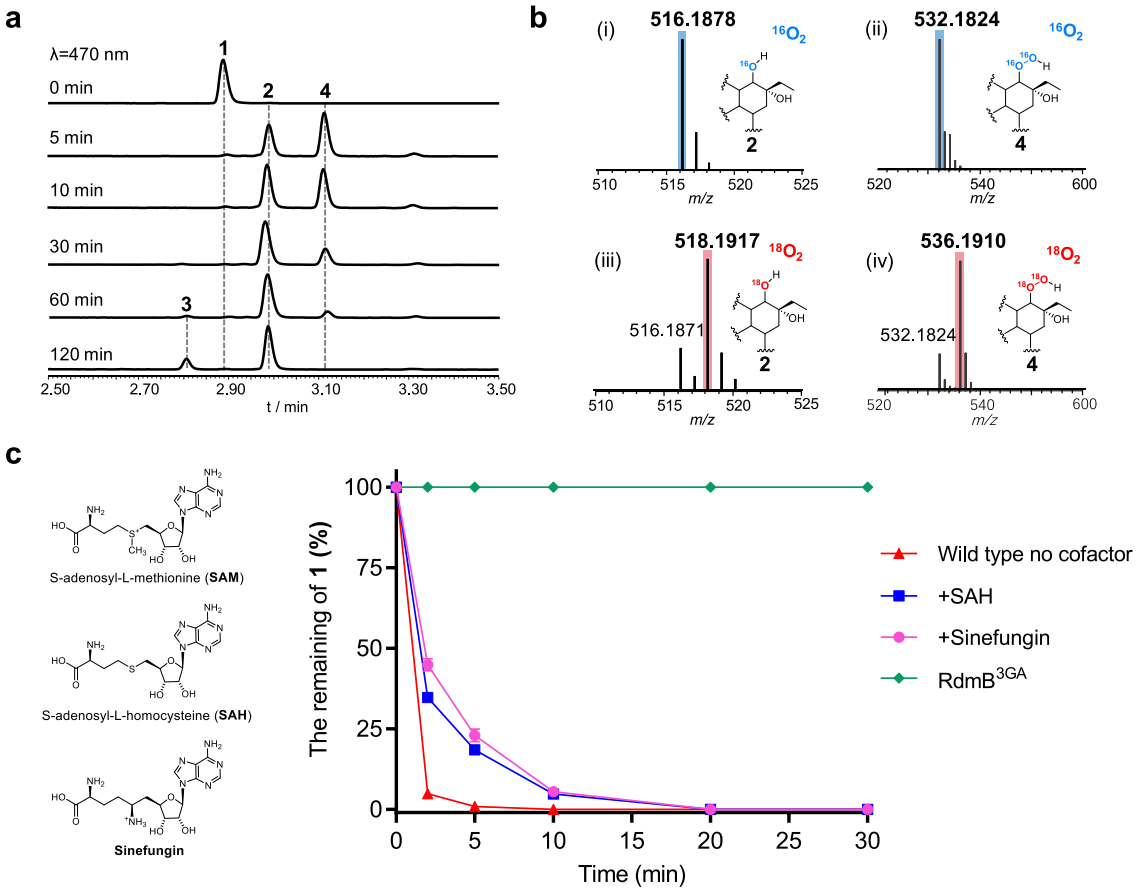

Fig. 2. Time-course analysis the conversion of **1** by RdmB catalyzed and the effect of SAM analogs on the catalytic reactions. (a) Time-course analysis of the conversion of **1** by RdmB in the presence of SAM. (b) HRESI-LCMS analysis of **2** and **4** delivered by RdmB in a mixture of $^{16}O_2$ (i and ii) and $^{18}O_2$ (iii and iv). (c) Time-course analysis of the consumption of **1** (50 μM) in the presence of RdmB (1 μM) with or without cofactors: SAM (200 μM), SAH (200 μM), Sinefungin (200 μM). The data show one representative experiment from at least three independent replicates.

iv). Thus, the oxygen atoms of **2** and **7** originated from O_2, which is consistent with the previously reported function of RdmB [10]. These results indicated that RdmB performs the two consecutive reactions in a stepwise mechanism, with the decarboxylative hydroxylation of **1** that produces the peroxide intermediate **4** occurring first, and then **4** undergoing homolytic cleavage of the O–O bond generating **2**, followed by the 4-*O*-methylation reaction forming **3**.

To further evaluate the catalytic properties of RdmB toward **1**, we determined the steady-state kinetic analysis by measuring the substrate consumption rates with HPLC. The result indicated that the k_{cat} and K_m values were 566.7 ± 23 min^{-1} and 12 ± 4.6 μM (Fig. S13), respectively, in the presence of SAM. This suggests that RdmB has a relatively efficient conversion rate to perform the hydroxylation and methylation reactions.

3.2. Role of SAM for RdmB

Methyl transfer is one of many biochemical processes requiring SAM as cofactor, and the positive charge of SAM may also be involved in the delocalization of electrons into the anthraquinone core of the substrate [27,28]. We next probed the involvement of SAM in catalyzing non-methylated reactions of RdmB. When the methyl donor SAM was removed from the RdmB reaction mixture, only led mainly to the production of **2** with a small ratio of the methylated product **3** (Fig. 1b–i). We reasoned that the low yield of **3** from **2** might be due to the co-purification of SAM with RdmB, which was demonstrated by the detecting SAM in the supernatant of heat-denatured RdmB by HRESI-LCMS analysis (Fig. S14) [20] and by using the SAM competitive inhibitor *S*-adenosyl-L-homocysteine (SAH, 400 μM) to reduce the production of **3** (Fig. S15) [29]. We then performed the RdmB enzymatic assays in the presence of the 200 μM SAH and 200 μM sinefungin [30], the conversion rate of **1** into the 10-hydroxylated product was affected slightly. In particular, the initial substrate conversion rate of **1** by RdmB was about 60 % and 50 % at 2 min when SAH or sinefungin was added, respectively, to the reaction mixture compared to the rate in the presence of SAM. Over time, substrate **1** was consumed by about 90 % at 10 min and completed at 20 min (Fig. 2c and S16). Furthermore, the three conserved glycine (G) residues in the SAM-binding motif (GXGXG) of RdmB were mutated to alanine (A) by site-directed mutagenesis to obtain the SAM-free protein RdmB^{3GA} (Figs. S4 and S14). However, the mutated RdmB^{3GA} completely abolished both the methylation and hydroxylation activities with **1** (Fig. 1b–iii). These results confirmed that the methylation and hydroxylation activities of RdmB are strictly dependent on the binding of SAM or its analogs. Given that SAH and sinefungin can also support the decarboxylative hydroxylation activity of RdmB, SAM and its analogs are considered an essential structural ligand to maintain ternary structural integrity and the proper binding mode and orientation of electron-rich substrates during decarboxylative hydroxylation of C-10 by RdmB.

3.3. Insights into the catalytic mechanism of RdmB

To study the catalytic mechanisms of RdmB, the three-dimensional crystal structure with **1** was performed. The X-ray crystal structures of RdmB-SAH-DOD was solved as homodimers at 2.2 Å resolution (PDB ID:

9J56), indicating that the decarboxylation and methylation reaction have proceeded during crystallization (Fig. 3a, Table S3). However, when DOC was used as substrate, the corresponding C-10 hydroxylated product was not detected (Fig. S11), suggesting that the substrate **1** may have undergone decarboxylation before entering the active site pocket of RdmB (Fig. S17). Each subunit of the single ternary structure displayed the typical fold of Class I methyltransferases, consisting of an *N*-terminal domain with a mainly helical structure for substrate recognition and dimerization and a *C*-terminus containing a Rossman-like fold for substrate binding and catalysis [31]. Specifically, the 10-decarboxylated and 4-*O*-methylated product DOD was found in the catalytic pocket, and SAH was bound to the consensus GxGxG located in a loop connecting the first β-sheet and the α-helix in the Rossman fold motif, close to DOD (Fig. 3a).

RdmB showed a distance of 4.6 Å between the C4 oxygen atom of DOD and the sulfur atom of SAH in the ternary complex structures (Fig. 3a, top). This distance range is suitable for hydrogen abstraction to form an *O*-methyl group, which also reasonably explains the methyltransferase activity of RdmB [27,28]. When substrate **1** was docked into the catalytic sites of RdmB by AutoDock Vina [26], one hydrogen bond was formed between RdmB N260 and the C4-hydroxyl group of **1** (Fig. S18), which may play important roles in the methylation activity. Additionally, a salt bridge was found between the side chains of RdmB R307 with the carbonyl group of **1,** which was proposed to be important for initiating the decarboxylative hydroxylation reaction (Fig. S18). Consequently, we conducted mutation studies of two key residues to further understand their roles in hydroxylation and methylation activities.

When RdmB^{N260A} was incubated with **1** in the presence of SAM, the production of hydroxylated **2,** but not the methylated product, was detected (Fig. 3b–ii). With compound **2** as substrate, the methylation activity of RdmB^{N260A} was completely abolished in the presence of SAM (Fig. S19). Accordingly, instead of the previously proposed "proximity and desolvation" mechanism [27,28,32], an Asn-mediated S_N2-like type methylation is suggested for RdmB, using an active N260 as a catalytic residue to deprotonate the C4 hydroxyl group of **1**. Deprotonation further enhances the nucleophilicity of the hydroxyl group to attack the SAM donor methyl group and contribute to rate acceleration of methylation. Our results also suggest that the C-7 triglycosylated substrate (*i.e.,* aclacinomycin A) prevents the proper binding mode needed to accommodate the potential proton extraction of the C4 hydroxyl group from the conserved Asn residue of RdmB, preventing methyl

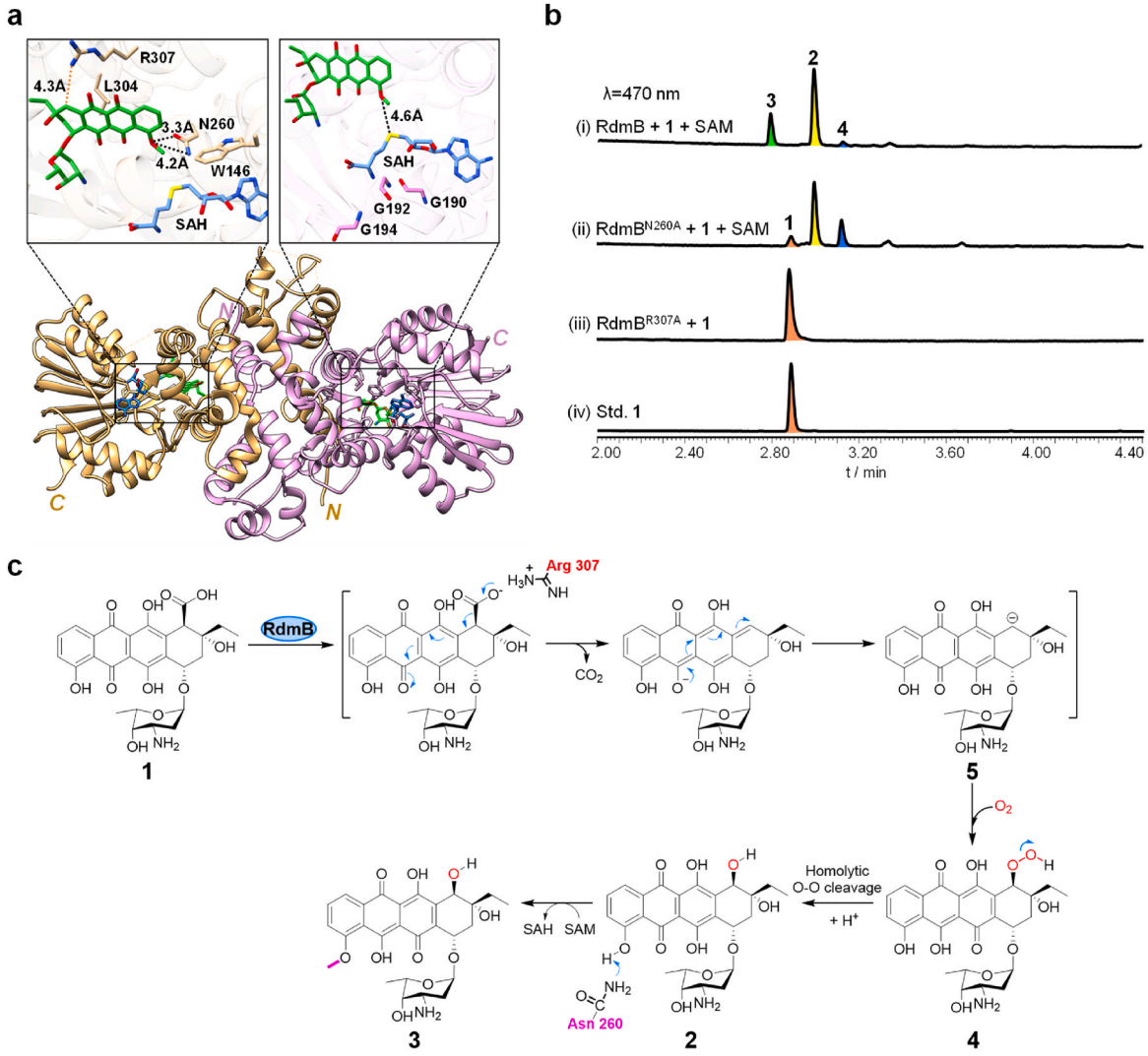

Fig. 3. Ternary complexe structure of RdmB with functional verification by sited-directed mutagenesis and Proposed catalytic mechanism of RdmB. (a) 3D structure of RdmB bound with product **3** and SAH. The two monomers of RdmB are colored in tan and lilac. The top box shows a zoom-in view of the active site of RdmB with **3**. (b) UPLC analysis of enzymatic conversion of **1** by RdmB site-directed mutants. (i) RdmB^{WT} in the presence of 1 mM SAM; (ii) RdmB^{N260A} in the presence of 1 mM SAM; (v) RdmB^{R307A}; (vi) Std. **1**: The standard of **1**. (c) Proposed catalytic mechanisms mediated by RdmB toward substrate **1**. Product **2** is derived by RdmB from homolytic O–O bond cleavage of the peroxyl intermediate **4** since no reductant was added into the reaction mixture.

transfer activity.

On the other hand, no conversion of **1** was detected with RdmB^{R307A} in the presence of SAM after 2 h, indicating that R307 is the key residue for the hydroxylation reaction (Fig. 3b–iii). Accordingly, substrate-assisted activation mechanisms of RdmB utilizing a highly-conjugated electron-rich tetracyclic 7,8,9,10-tetrahydro-5,12-naphtacenoquinone moiety were proposed [27,28,33,34]. After **1** binds to the RdmB catalytic pocket, decarboxylation of **1** is initiated by R307 in the presence of SAM, resulting in the formation of the carbanion intermediate **5**. Subsequently, substrate-assisted activation of O_2 oxidizes **5** to yield the hydroperoxide intermediate **4**, which is then converted into **2** by spontaneous homolytic O–O bond cleavage, followed by the 4-*O*-methylation reaction forming **3** (Fig. 3c).

4. Conclusion

We demonstrated the inherent 4-*O*-methylation activity of RdmB in anthracycline biosynthesis. Based on our comparative analysis, a new Asn-mediated acid/base catalyzed S_N2-type nucleophilic substitution methylation by RdmB was proposed instead of the previously reported "proximity and desolvation" mechanism. RdmB activity is cofactor dependent and stepwise. Furthermore, the 10-OH group introduced by RdmB originates from O_2.

Several SAM-dependent methyltransferases can catalyze diverse types of non-methylating reactions [35–39]. Interestingly, methyltransferase TnmJ, involved in anthraquinone-fused enediyne biosynthesis, functions as an oxygenase in catalyzing deformylation and epoxidation reactions [40]. Our functional characterization of RdmB expands our understanding of the versatility and potential of methyltransferases.

Data availability statement

The data that support the findings of this study are available in the supplementary material of this article.

CRediT authorship contribution statement

Moli Sang: Writing – original draft, Methodology, Data curation, Conceptualization. **Qingyu Yang:** Validation, Software, Conceptualization. **Jiawei Guo:** Software, Conceptualization. **Peiyuan Feng:** Validation, Conceptualization. **Wencheng Ma:** Validation, Conceptualization. **Wei Zhang:** Writing – review & editing, Writing – original draft, Validation, Supervision, Resources, Project administration, Methodology, Investigation, Funding acquisition, Data curation, Conceptualization.

Declaration of competing interest

The authors declare that they have no known competing financial interests or personal relationships that could have appeared to influence the work reported in this paper.

Acknowledgments

This work was supported by the National Key Research and Development Program of China (2019YFA0905400 and 2019YFA0905700), the National Natural Science Foundation of China (U2106227 and 82022066), the Shandong Provincial Natural Science Foundation (ZR2021ZD28), and the Shenzhen Fundamental Research Program (20220523121619003). We also thank Guannan Lin, Jing Zhu, Zhifeng Li, Jingyao Qu, and Haiyan Sui of the Core Facilities for Life and Environmental Sciences, State Key laboratory of Microbial Technology of Shandong University for HRESI-LCMS and NMR analysis.

Appendix A. Supplementary data

Supplementary data to this article can be found online at https://doi.org/10.1016/j.synbio.2024.09.002.

References

[1] Krohn K. Anthracycline chemistry and biology I: biological occurrence and biosynthesis, synthesis and chemistry, vol. 282. Springer; 2009.
[2] Geneviève AS, Danielle LG. Daunorubicin and doxorubicin, anthracycline antibiotics, a physicochemical and biological review. Biochimie 1984;66(5):333–52. https://doi.org/10.1016/0300-9084(84)90018-x.
[3] Warrell Jr RP. Aclacinomycin A: clinical development of a novel anthracycline antibiotic in the haematological cancers. Drugs Exp Clin Res 1986;12(1):275–82. https://doi.org/10.1016/0300-9084(84)90018-x.
[4] Cersosimo RJ, Hong WK. Epirubicin: a review of the pharmacology, clinical activity, and adverse effects of an adriamycin analogue. J Clin Oncol 1986;4(3):425–39. https://doi.org/10.1200/jco.1986.4.3.425.
[5] Wang Y, Niemi J, Airas K, Ylihonko K, Hakala J, Mäntsälä P. Modifications of aclacinomycin T by aclacinomycin methyl esterase (RdmC) and aclacinomycin-10-hydroxylase (RdmB) from *Streptomyces purpurascens*. Biochim Biophys Acta 2000;1480(1–2):191–200. https://doi.org/10.1016/s0167-4838(00)00089-3.
[6] Grocholski T, Dinis P, Niiranen L, Niemi J, Mikko MK. Divergent evolution of an atypical *S*-adenosyl-L-methionine-dependent monooxygenase involved in anthracycline biosynthesis. Proc Natl Acad Sci U S A 2015;112(32):9866–71. https://doi.org/10.1073/pnas.1501765112.
[7] Hulst MB, Grocholski T, Neefjes JJC, Wezel GP van, Ketela MM. Anthracyclines: biosynthesis, engineering and clinical applications. Nat Prod Rep 2022;39(4):814–41. https://doi.org/10.1039/d1np00059d.
[8] Hertweck C, Luzhetskyy A, Rebets Y, Bechthold A. Type II polyketide synthases: gaining a deeper insight into enzymatic teamwork. Nat Prod Rep 2007;24(1):162–90. https://doi.org/10.1039/b507395m.
[9] Niemi J, Mäntsälä P, Niemi J, Mäntsälä P. Nucleotide sequences and expression of genes from *Streptomyces purpurascens* that cause the production of new anthracyclines in *Streptomyces galilaeus*. J Bacteriol 1995;177(10):2942–5. https://doi.org/10.1128/jb.177.10.2942-2945.1995.
[10] Jansson A, Koskiniemi H, Erola A, Wang J, Mäntsälä P, Schneider G, et al. Aclacinomycin 10-hydroxylase is a novel substrate-assisted hydroxylase requiring *S*-adenosyl-L-methionine as cofactor. J Biol Chem 2005;280(5):3636–44. https://doi.org/10.1074/jbc.M412095200.
[11] Jansson A, Niemi J, Lindqvist Y, Mäntsälä P, Schneider G. Crystal structure of aclacinomycin-10-hydroxylase, a S-adenosyl-L-methionine-dependent methyltransferase homolog involved in anthracycline biosynthesis in *Streptomyces purpurascens*. J Mol Biol 2003;334(2):269–80. https://doi.org/10.1016/j.jmb.2003.09.061.
[12] Dinis P, Tirkkonen H, Wandi BN, Siitonen V, Niemi J, Grocholski T, et al. Evolution-inspired engineering of anthracycline methyltransferases. Proc Natl Acad Sci Nexus 2023;2(2):1–10. https://doi.org/10.1093/pnasnexus/pgad009.
[13] Struck AW, Thompson ML, Wong LS, Micklefield J. *S*-adenosyl-methionine-dependent methyltransferases: highly versatile enzymes in biocatalysis, biosynthesis and other biotechnological applications. Chembiochem 2012;13(18):2642–55. https://doi.org/10.1002/cbic.201200556.
[14] Dickens ML, Priestley ND, Strohl WR. *In vivo* and *in vitro* bioconversion of epsilon-rhodomycinone glycoside to doxorubicin: functions of DauP, DauK, and DoxA. J Bacteriol 1997;179(8):2641–50. https://doi.org/10.1128/jb.179.8.2641-2650.1997.
[15] Blumauerová M, Matějů J, Stajner K, Vaněk Z. Studies on the production of daunomycinone-derived glycosides and related metabolites in *Streptomyces coeruleorubidus* and *Streptomyces peucetius*. Folia Microbiol 1977;22(4):275–85. https://doi.org/10.1007/bf02877657.
[16] Robert X, Gouet P. Deciphering key features in protein structures with the new ENDscript server. Nucleic Acids Res 2014;42:320–4. https://doi.org/10.1093/nar/gku316.
[17] Notredame C, Higgins DG, Heringa J. T-Coffee: a novel method for fast and accurate multiple sequence alignment. J Mol Biol 2000;302(1):205–17. https://doi.org/10.1006/jmbi.2000.4042.
[18] Huang H, Zheng G, Jiang W, Hu HF, Lu YH. One-step high-efficiency CRISPR/Cas9-mediated genome editing in *Streptomyces*. Acta Biochim Biophys Sin 2015;47(4):231–43. https://doi.org/10.1093/abbs/gmv007.
[19] Kieser T, Bibb MJ, Buttner MJ, Chater KF, Hopwood DA. Practical streptomyces genetics, vol. 291. John Innes Foundation Norwich; 2000.
[20] Iwig DF, Booker SJ. Insight into the polar reactivity of the onium chalcogen analogues of *S*-adenosyl-L-methionine. Biochemistry 2004;43(42):13496–509. https://doi.org/10.1021/bi048693.
[21] Minor W, Cymborowski M, Otwinowski Z, Chruszcz M. HKL-3000: the integration of data reduction and structure solution-from diffraction images to an initial model in minutes. Acta Crystallogr D Biol Crystallogr 2006;62(8):859–66. https://doi.org/10.1107/s0907444906019949.
[22] Emsley P, Cowtan K. Coot: model-building tools for molecular graphics. Acta Crystallogr 2004;60(12):2126–32. https://doi.org/10.1107/s0907444904019158.
[23] Adams PD, Afonine PV, Bunkóczi G, Chen VB, Davis IW, Echols N, et al. PHENIX: a comprehensive Python-based system for macromolecular structure solution. Acta Crystallogr 2010;66(2):213–21. https://doi.org/10.1107/s0907444909052925.

[24] Davis IW, Andrew LF, Chen VB, Block JN, Kapral GJ, Wang X, et al. MolProbity: all-atom contacts and structure validation for proteins and nucleic acids. Nucleic Acids Res 2007;35:375–83. https://doi.org/10.1093/nar/gkm216.
[25] Pettersen EF, Goddard TD, Huang CC, Huang CC, Meng EC, Couch GS, et al. UCSF ChimeraX: structure visualization for researchers, educators, and developers. Protein Sci 2021;30(1):70–82. https://doi.org/10.1002/pro.3943.
[26] Morris GM, Huey R, Lindstrom W, Sanner MF, Belew RK, Goodsell DS, et al. AutoDock4 and AutoDockTools4: automated docking with selective receptor flexibility. J Comput Chem 2009;30(16):2785–91. https://doi.org/10.1002/jcc.21256.
[27] Sun Q, Huang M, Wei Y. Diversity of the reaction mechanisms of SAM-dependent enzymes. Acta Pharm Sin B 2021;11(3):632–50. https://doi.org/10.1016/j.apsb.2020.08.011.
[28] Lee YH, Ren D, Jeon B, Liu HW. *S*-Adenosylmethionine: more than just a methyl donor. Nat Prod Rep 2023;40(9):1521–49. https://doi.org/10.1039/d2np00086e.
[29] Coward JK, Slisz EP. Analogs of S-adenosylhomocysteine as potential inhibitors of biological transmethylation. Specificity of the S adenosylhomocysteine binding site. J Med Chem 1973;16(5):460–3. https://doi.org/10.1021/jm00263a008.
[30] Bauer NJ, Kreuzman AJ, Dotzlaf JE, Yeh WK. Purification, characterization, and kinetic mechanism of *S*-adenosyl-L-methionine:macrocin O-methyltransferase from *Streptomyces fradiae*. J Biol Chem 1988;263(30):15619–25. https://doi.org/10.1016/S0021-9258(19)37633-1.
[31] Liscombe DK, Louie GV, Noel JP. Architectures, mechanisms and molecular evolution of natural product methyltransferases. Nat Prod Rep 2012;29(10):1238–50. https://doi.org/10.1039/c2np20029e.
[32] Jansson A, Koskiniemi H, Mäntsälä P, Niemi J, Schneider G. Crystal structure of a ternary complex of DnrK, a methyltransferase in daunorubicin biosynthesis, with bound products. J Biol Chem 2004;279(39):41149–56. https://doi.org/10.1074/jbc.m407081200.
[33] Siitonen V, Blauenburg B, Kallio P, Mäntsälä P, Mikko MK. Discovery of a two-component monooxygenase SnoaW/SnoaL2 involved in nogalamycin biosynthesis. J Biol Chem 2012;19(5):638–46. https://doi.org/10.1016/j.chembiol.2012.04.009.
[34] Machovina MM, Usselman RJ, DuBois JL. Monooxygenase substrates mimic flavin to catalyze cofactorless oxygenations. J Biol Chem 2016;291(34):17816–28. https://doi.org/10.1074/jbc.m116.730051.
[35] Awakawa T, Zhang L, Wakimoto T, Hoshino S, Mori T, Ito T, et al. A methyltransferase initiates terpene cyclization in teleocidin B biosynthesis. J Am Chem Soc 2014;136(28):9910–3. https://doi.org/10.1021/ja505224r.
[36] Yu F, Li M, Xu C, Sun B, Zhou H, Wang Z, et al. Crystal structure and enantioselectivity of terpene cyclization in SAM-dependent methyltransferase TleD. Biochem J 2016;473(23):4385–97. https://doi.org/10.1042/bcj20160695.
[37] Huang C, Smith CV, Glickman MS, Jacobs WR, Sacchettini JC. Crystal structures of mycolic acid cyclopropane synthases from Mycobacterium tuberculosis. J Biol Chem 2002;277(13):11559–69. https://doi.org/10.1074/jbc.m111698200.
[38] Ohashi M, Liu F, Hai Y, Chen M, Tang MC, Yang Z, et al. SAM-dependent enzyme-catalysed pericyclic reactions in natural product biosynthesis. Nature 2017;549(7673):502–6. https://doi.org/10.1038/nature23882.
[39] Chang Z, Ansbacher T, Zhang L, Yang Y, Ko TP, Zhang G, et al. Crystal structure of LepI, a multifunctional SAM-dependent enzyme which catalyzes pericyclic reactions in leporin biosynthesis. Org Biomol Chem 2019;17(8):2070–6. https://doi.org/10.1039/c8ob02758g.
[40] Gui C, Kalkreuter E, Liu YC, Li G, Steele AD, Yang D, et al. Cofactorless oxygenases guide anthraquinone-fused enediyne biosynthesis. Nat Chem Biol 2024;20(2):243–50. https://doi.org/10.1038/s41589-023-01476-2.